RMetS
Royal Meteorological Society

Dependence of tropical-cyclone intensification on the boundary-layer representation in a numerical model

Roger K. Smith* and Gerald L. Thomsen
Meteorological Institute, University of Munich, Munich, Germany
*Correspondence to: Roger K. Smith, Meteorological Institute, University of Munich, Theresienstrasse 37, 80333 Munich, Germany. E-mail: roger.smith@lmu.de

We present idealized numerical model experiments to investigate the dependence of tropical-cyclone intensification and, in particular, the kinematic structure of the tropical-cyclone boundary layer on the boundary-layer parametrization in the model. The study is motivated by recent findings highlighting the important dynamical role of the boundary layer in tropical-cyclone intensification. The calculations are carried out using the Pennsylvania State University–National Center for Atmospheric Research fifth-generation mesoscale model (MM5). Predictions using one of five available schemes are compared, not only between themselves, but where possible with recent observational analyses of boundary-layer structure. At this stage the study falls short of being able to advocate the use of a particular scheme, although certain shortcomings of individual schemes are identified. The current inability to determine 'the optimum scheme' has implications for the predictability of tropical-cyclone intensification.

Key Words: hurricane; typhoon; vortex intensification

Received 21 April 2010; Revised 16 July 2010; Accepted 20 July 2010; Published online in Wiley Online Library 27 September 2010

Citation: Smith RK, Thomsen GL. 2010. Dependence of tropical-cyclone intensification on the boundary-layer representation in a numerical model. *Q. J. R. Meteorol. Soc.* **136**: 1671–1685. DOI:10.1002/qj.687

1. Introduction

The boundary layer* of a mature hurricane has been long recognized to be an important feature of the storm. In the 1960s, the frictionally induced inflow that occurs there was seen to be necessary to sustain the storm by supplying moisture to 'fuel' the eyewall clouds (Riehl and Malkus, 1960). However, subsequent studies suggested a more dynamic role wherein the boundary layer supplies the storm also with absolute angular momentum† M (Emanuel, 1986, 1997). Even so, the conventional view of tropical-cyclone spin-up continued to invoke the need for the radial convergence of M above the boundary layer, where M is approximately conserved. The convergence is produced by increasing system-scale radial buoyancy‡ gradients associated with deep, inner-core convection in the presence of enhanced surface moisture fluxes. This mechanism has been articulated previously by many authors (Ooyama, 1969, 1982; Willoughby, 1988, 1995). One exception is the idealized time-dependent model proposed by Emanuel (1997) in which the spin-up process, accompanied by the contraction of the eyewall, is determined entirely by the boundary layer, apparently without the need for convergence of M above the boundary layer.

*We use the term 'boundary layer' here to describe the shallow layer of strong inflow near the sea surface that is typically 500 m to 1 km deep and that arises largely because of the frictional disruption of gradient-wind balance near the surface. Alternative definitions based on thermodynamic considerations are discussed in Smith and Montgomery (2010).

†The absolute angular momentum is related to the azimuthally averaged tangential wind speed, v, by the formula $v = M/r - \frac{1}{2}fr$, where r is the radius of an air parcel from the vortex centre and f is the Coriolis parameter. In the absence of friction, M is a materially conserved quantity, so that both terms in the above expression lead to an increase in v as r decreases, and conversely.

‡The concepts of system-scale and local buoyancy in rapidly rotating vortices are discussed by Smith *et al.* (2005).

1.1. Recent theoretical insights

Recently, Smith *et al.* (2009; henceforth M3) revisited the problem of interpreting the dynamics of tropical-cyclone intensification in a three-dimensional numerical model. They showed that, from an azimuthally-averaged viewpoint, there are two mechanisms for vortex intensification, both involving the radial convergence of M. The first mechanism is associated with the radial convergence of M *above the boundary layer* induced by inner-core convection as described above. It explains why the vortex expands in size and may be interpreted in terms of balanced dynamics (Bui *et al.* 2009).

The second mechanism is associated with the radial convergence of M *within the boundary layer* and becomes important in the inner core. Although M is *not* materially conserved in the boundary layer, the largest wind speeds anywhere in the vortex can be achieved in or at the top of the boundary layer. This happens if the radial inflow is sufficiently large to bring air parcels to small radii with a minimal loss of angular momentum (in other words the reduction of M in the formula for v is more than offset by the reduction in r).[§] This mechanism explains why the maximum azimuthally-averaged tangential wind speeds in the model calculations of M3 and in those of other authors (e.g. Zhang *et al.* 2000) are located at low levels near the top of the boundary layer. The statement in Smith *et al.* (2009) that these mechanisms are independent is too strong: there must be a degree of coupling between them through boundary-layer dynamics. Thus, if the inner-core convection leads to an increase in tangential wind speed above the boundary layer by the first mechanism then the boundary-layer inflow will increase, leading to further spin-up of the vortex core by the second mechanism.

1.2. Importance for the boundary layer

The foregoing theoretical results show that *the spin-up of the vortex core is tied fundamentally to the dynamics of the boundary layer* and indicate the central importance of the boundary layer and its representation in numerical models for the prediction of tropical-cyclone intensification. In view of this finding, it is natural to ask how well boundary-layer processes are represented in tropical-cyclone forecast models. Several boundary-layer schemes have been proposed for use in such models, but these have been mostly formulated and calibrated to characterize the convective boundary layer over land. Their validity in the strong-wind region of hurricanes has not been firmly established, especially in the region where the boundary layer separates to feed the eyewall clouds (Smith and Montgomery, 2010). From a modelling perspective the question arises: *what is the most appropriate scheme for predicting tropical-cyclone intensification*?

1.3. Previous appraisals of boundary-layer schemes

An early study demonstrating the importance of resolving the tropical-cyclone boundary layer was that by Anthes and Chang (1978), who compared a hurricane simulation in a model with relatively high resolution in the boundary layer with one in which the boundary layer was treated as a single layer. They found that the extra resolution of the boundary layer affected the behaviour of the simulated storms and their sensitivity to changes in surface properties, although their structures above the boundary layer were similar. The study raised questions about the sensitivity of more sophisticated, higher-resolution models to the boundary-layer parametrization and whether some parametrization schemes might be more predisposed toward developing strong hurricanes than others.

Motivated by the above question, Braun and Tao (2000) carried out high-resolution simulations of *Hurricane Bob* (1991) using the MM5 model (Dudhia, 1993; Grell *et al.*, 1995). Tests were conducted to determine the sensitivity of the simulation to four planetary boundary-layer parametrizations in the model, including the bulk aerodynamic, Blackadar, medium-range forecast (MRF) model and Burk–Thompson schemes. Significant sensitivity was found between the calculations, with maximum winds varying by 15 m s^{-1}, but all of the calculations overestimated the observed intensity of the storm. At the time of their study, the boundary layer was thought of mainly as providing the moisture source to fuel the eyewall convection. However, following the findings of M3, it is seen as playing a direct dynamical role in the spin-up process, a recognition that calls for a more comprehensive reappraisal of different boundary-layer parametrizations with a particular focus on the processes articulated in M3.

BT00 chose to assess different boundary-layer schemes in a single case study, presumably with a view to identifying the most skillful scheme. However, it turned out than none of the schemes reproduced the intensification of *Hurricane Bob* especially well. A similar case study has been carried out recently by Nolan *et al.* (2009a,b), who examined two boundary-layer schemes in the Weather Research and Forecasting Model (WRF), the Yonsei University and the Mellor–Yamada–Janjić schemes. They examined also two modifications of these schemes. Their study focussed on the mature hurricane stage and the main conclusion seemed to be that, although there were many differences in detail between the schemes, all the simulations were 'in good agreement with the detailed analyses of in-situ data'. Notably, the study fell short of recommending a particular scheme, although it did caution that a particular scheme might be sensitive to the model in which it used. Hill and Lackmann (2009) studied also these boundary-layer schemes in the WRF model, but in an idealized calculation. They attributed the differences between the schemes to the differences in the exchange coefficients.

A recent assessment of the state-of-the-art Advanced Hurricane Weather Research and Forecasting model (HWRF) by Davis *et al.* (2007) examined, *inter alia*, the sensitivity of predictions of *Hurricane Katrina* (2005) to the model resolution and the formulation of surface-momentum exchange. Interestingly, it did not consider that

[§]An alternative, but equivalent, interpretation for the material acceleration of the mean tangential wind follows directly from Newton's second law in which, for an inviscid, axisymmetric flow, the sole force is the generalized Coriolis force, $-u(v/r+f)$, where u is the mean radial velocity component. If the flow is convergent, $u<0$, so that this force is positive and leads to an acceleration of v. If friction is present, but if rings of air converge quickly enough (i.e. if u is sufficiently large), the generalized Coriolis force can exceed the tangential component of frictional force and the tangential winds will increase with decreasing radius in the boundary layer as well. It is precisely for this reason that supergradient winds can arise in the boundary layer (Nguyen *et al.*, 2002; Smith and Vogl, 2008).

there might also be a sensitivity also to the boundary-layer parametrization used in the model. This omission reflects our experience in talking with model developers that the choice of boundary-layer parametrization is low on the list of priorities when designing models for the prediction of tropical cyclones: in several instances the modeller had to go away and check exactly which scheme was in use! In view of this situation, and in the light of the theoretical results described above indicating the important role of boundary-layer dynamics and thermodynamics on tropical-cyclone spin-up, we present here a further comparison of different boundary-layer schemes in the tropical-cyclone context.

1.4. *The present study*

Here we investigate the dependence of vortex spin-up on the choice of the boundary-layer parametrization scheme in idealized numerical model simulations. This approach has the advantage that *it avoids many of the complications inherent in studies of individual cases with full-physics models*, although *it does not alleviate the difficulties of making detailed comparisons with observations*. The calculations are based on the thought experiment discussed by Nguyen *et al.* (2008; henceforth M1), which considers the spin-up of an initially symmetric vortex on an f-plane in a quiescent environment. Like Nguyen *et al.*, we use the MM5 model, but here we compare five boundary-layer schemes available in the model.[¶]

In this study we focus exclusively on dynamical aspects of the boundary layer in the intensification process as predicted by the different schemes: thermodynamical aspects of the schemes, which are undoubtedly important, will be discussed in a separate article. Where possible, we compare the low-level wind structure predicted by schemes with observations of Franklin *et al.* (2003), Kepert (2006a,b) and Bell and Montgomery (2008). While these comparisons fall short of enabling us to determine 'the optimum scheme' for reasons discussed later, they do allow us to determine the range of variation of vortex structure and intensity between different schemes. For this reason, *the calculations have implications for the predictability of tropical-cyclone intensity*.

The article is organized as follows. The numerical experiments are described in section 2, including the derivation of initial conditions and modifications to some of the model physics. Section 2.1 provides a brief description of boundary-layer schemes, of which more details are given in an appendix. The results are described in sections 3 and a discussion of these is the subject of section 4. The conclusions are given in section 5.

2. The model configuration

The numerical experiments are similar to those described in M1. They are carried out using a modified version of MM5 (version 3.6). The model is configured with three domains: a coarse mesh with a 45 km horizontal grid size and two two-way nested domains with grid sizes 15 and 5 km. The domains are square and are 9000 km, 4500 km, 1500 km on each side. There are 24 σ-levels in the vertical, 10 of which are below 850 mb. The model top is at a pressure of 50 mb. The calculations are performed on an f-plane centred at 20°N.

Deep moist convection is resolved explicitly and represented by the warm-rain scheme as used in section 5 of M1. In addition we use one of five boundary-layer schemes as detailed in subsection 2.1. The warm-rain and boundary-layer schemes are applied in all domains. The sea surface temperature is a constant (27 °C). We use the simplest radiative cooling scheme available in MM5, which imposes a temperature-dependent cooling rate of the order of 1–2 °C day^{-1}.

The initial vortex is axisymmetric with a maximum tangential wind speed of 15 m s^{-1} at the surface at a radius of 120 km. The magnitude of the tangential wind decreases sinusoidally with height, vanishing at the top model level. The temperature field is initialized to be in gradient-wind balance with the wind field using the method described by Smith (2006). The far-field temperature and humidity are based on Jordan's Caribbean sounding for the hurricane season (Jordan, 1958).

For the purpose of calculating azimuthal averages, the vortex centre is defined as the centroid of relative vorticity at 900 mb over a circular region of 200 km radius from a 'first-guess' centre, which is determined by the minimum of the total wind speed at 900 mb.

2.1. *The boundary-layer schemes*

The five boundary-layer schemes examined are listed in Table I together with a brief description of each. Further details are given in an appendix. In the five main calculations, the surface drag and heat and moisture-exchange coefficients are modified in line with the results of the coupled boundary-layer air–sea transfer experiment (CBLAST: see Black *et al.*, 2007). The surface-exchange coefficients for sensible heat and moisture are set to the same constant, 1.2×10^{-3}, and that for momentum, the drag coefficient, is set to $0.7 \times 10^{-3} + 1.4 \times 10^{-3}[1 - \exp(-0.055|\mathbf{u}|)]$, where $|\mathbf{u}|$ is the wind speed at the lowest model level. Use of the same formulation in each scheme facilitates a proper comparison of the schemes. Two additional calculations are described briefly in which the bulk scheme and Gayno–Seaman scheme are used with the default values (see appendix) for their surface-exchange coefficients to assess the impact of changing these coefficients.

3. Results

3.1. *Time evolution*

Figure 1 shows time series of the maximum azimuthally-averaged tangential wind component, ($v_{\max}$), and the maximum azimuthally averaged radial inflow and outflow components, ($u_{\min}$ and $u_{\max}$), in the lowest 3 km in the set of five calculations with different boundary-layer parametrizations (labelled 1–5). Time series of $v_{\max}$ are also shown for the bulk and Gayno–Seaman schemes with their default surface-exchange coefficients (labelled 6 and 7, respectively). All the time series exhibit considerable variability and have been smoothed by applying a 1–2–1 filter four times. As judged by the maximum azimuthally averaged tangential wind speed, the earliest onset of rapid intensification occurs in the two bulk schemes and the two Gayno–Seaman schemes (Figure 1(a) and (b)). Rapid

[¶]Nguyen *et al.* used the bulk aerodynamic scheme.

Table I. Boundary-layer schemes used in this study with a brief description of each scheme. Versions of the bulk scheme and Gayno–Seaman scheme with their default values for the exchange coefficients are studied also.

No.	Scheme	Brief description
1	bulk	Surface fluxes of sensible heat, latent heat and momentum determined by a bulk-aerodynamic formula. Fluxes within the boundary layer calculated by a first-order (local K-mixing) scheme.
2	Blackadar	Vertical transfer of momentum, heat and moisture is determined by (non-local) transilient mixing in the free convective state. The surface layer fluxes are based on Monin–Obukhov similarity theory.
3	Burk–Thompson	Mellor-Yamada level 2.5 with turbulent kinetic energy (TKE) prediction. The eddy-exchange coefficient of an adiabatically conserved quantity is related to the calculated TKE. The Louis (1979) scheme is used to parametrize the surface layer. "
4	MRF	Local k-mixing with countergradient correction of q and θ in the free convective state. The surface layer fluxes are based on Monin–Obukhov similarity theory.
5	Gayno–Seaman	Mellor-Yamada level 2.5 with TKE prediction, including horizontal and vertical advection and horizontal diffusion of TKE. The eddy-exchange coefficient of an adiabatically conserved quantity is related to the predicted TKE. A countergradient correction is applied to the liquid-water potential temperature in the free convective state. Surface layer fluxes are based on Monin–Obukhov similarity theory.

intensification in the other calculations occurs 6–12 hours later, except in the MRF scheme where the intensification rate is much more sluggish. With this scheme, the vortex takes more than a day longer to reach hurricane strength ($33\,\mathrm{m\,s^{-1}}$) than with the bulk scheme. However, it continues to intensify steadily, even at 120 hours, while the other schemes have reached a quasi-steady state at this time. Because of close similarities between the modified and unmodified Gayno–Seaman schemes, we do not discuss the unmodified version further.

The unmodified bulk scheme (curve 6 in Figure 1(b)) gives the largest intensity with v_{max} just over $85\,\mathrm{m\,s^{-1}}$ although, in the light of the findings of M1,[‖] one would judge that there is little significant difference in intensification between the two bulk schemes during much of the integration (Figure 1(b)). With the other schemes, v_{max} lies in the range 58–68 $\mathrm{m\,s^{-1}}$. The differences between the v_{max} curves for the Blackadar, Burk–Thompson and modified Gayno–Seaman schemes are barely significant (see footnote below) for the first 100 hours of the calculation (Figure 1(a)) and between the two bulk schemes and the unmodified Gayno–Seaman scheme for 63 hours of integration (Figure 1(b)). The difference in intensity after five days between the seven calculations is about $20\,\mathrm{m\,s^{-1}}$.

The foregoing results are slightly different from those of BT00, who found that, after 72 hours of integration, the Burk–Thompson and bulk schemes produced the strongest storms and the MRF scheme the weakest one (in our calculations, the MRF scheme also gives the weakest storm during the first 72 hours). The intensity differences between schemes are comparable with those reported by BT00, who found differences reaching up to $22\,\mathrm{m\,s^{-1}}$ during the integration. It is pertinent to recall that, in the main comparison of schemes described in BT00, section 4, the schemes had different surface-exchange coefficients.

The maximum inflow and outflow also show considerable differences between the five schemes (panels (c) and (d) of Figure 1). These quantities were not shown by BT00, but following the work of M3 are considered to be important. During the period of rapid intensification, the largest inflow occurs for the modified bulk scheme, with the speed reaching $37\,\mathrm{m\,s^{-1}}$ just before 108 hours and then decreasing a little. By far the weakest inflow occurs in the MRF scheme, with the speed reaching only $17\,\mathrm{m\,s^{-1}}$. The Blackadar, Burk–Thompson and Gayno–Seaman schemes have maximum radial inflow speeds after 5 days of about $24\,\mathrm{m\,s^{-1}}$. In broad terms, the inflow velocity component is important as its strength and spatial distribution determine how close to the rotation axis air parcels can penetrate in the boundary layer. This distance influences how fast they may spin, another factor being the amount of absolute angular momentum lost by friction. An alternative view is that, since the advective contribution to the total tangential wind tendency is dominated by the radial advection of absolute vorticity, the spin-up rate is intimately coupled with the radial wind component (Bui *et al.*, 2009, figure 9). The maximum outflow shown in panel (d) of Figure 1 is discussed in the next section.

3.2. *Mature-stage wind structure*

The differences in the wind structure between the five boundary-layer schemes (including both versions of the bulk scheme) are highlighted by radius–height cross-sections of azimuthally-averaged radial and tangential wind components in the lowest 3 km. Figure 2 shows such cross-sections with the fields averaged between 108 and 120 hours of integration. In this period all vortices, except that for

[‖] M1 noted that deep convective cores containing enhanced low-level rotation are the coherent structures of the intensification process and that the details of these structures are sensitive to the low-level moisture distribution. For this reason they carried out a series of ensemble calculations to examine the sensitivity of the control calculation to small randomly distributed perturbations of the initial moisture in the lowest 100 mb and found a spread in the calculated intensity between ensemble members at any given time. This spread has a standard deviation of the order of $\pm 7\,\mathrm{m\,s^{-1}}$ during the period of rapid intensification. They concluded that any differences in intensity between two deterministic calculations smaller than this amount were not significant.

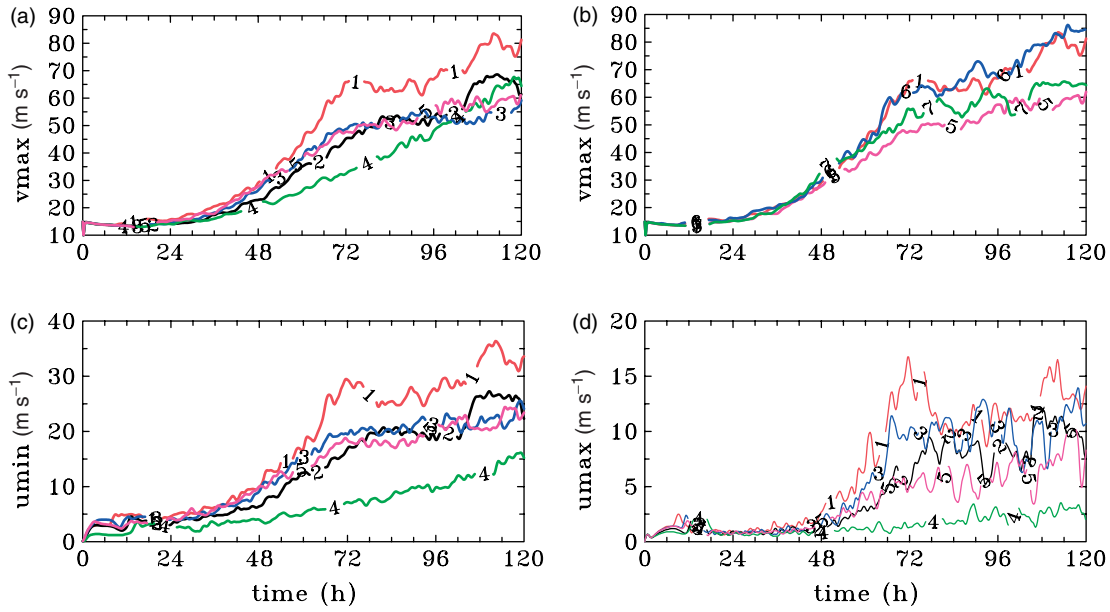

Figure 1. Time series: (a), (b) maximum azimuthally-averaged tangential wind speed, (c) minimum azimuthally-averaged radial wind speed *with the sign reversed* and (d) maximum azimuthally-averaged radial wind speed in the lowest 3 km in a set of calculations with different boundary-layer parametrizations: 1 = modified bulk scheme, 2 = Blackadar scheme, 3 = Burk–Thompson scheme, 4 = MRF scheme, 5 = Gayno–Seaman scheme, 6 = unmodified bulk scheme, 7 = unmodified Gayno–Seaman scheme (unmodified means with their default exchange coefficients). Note the different scales on the ordinate of each panel.

Table II. Maximum azimuthally-averaged tangential wind component (v_{max}), maximum and minimum azimuthally-averaged radial wind components (u_{max}, u_{min}) and maximum azimuthally-averaged total wind speed (V_{tmax}) averaged over the period 108–120 hours together with the radii ($r_{v_{max}}$, $r_{u_{max}}$, $r_{u_{min}}$, $r_{V_{tmax}}$) and heights ($z_{v_{max}}$, $z_{u_{max}}$, $z_{u_{min}}$, $z_{V_{tmax}}$) at which they occur for the five boundary-layer schemes, including the modified and unmodified versions of the bulk scheme, as indicated.

Scheme	Mod bulk	Unmod bulk	Blackadar	Burk–Thompson	MRF	Gayno–Seaman
v_{max} (m s^{-1})	79.4	82.6	66.4	54.2	62.4	58.2
$r_{v_{max}}$ (km)	28	32	40	52	52	48
$z_{v_{max}}$ (km)	0.6	0.5	0.7	0.9	1.4	0.9
u_{min} (m s^{-1})	−33.5	−29.4	−25.8	−22.5	−13.8	−22.0
$r_{u_{min}}$ (km)	36	40	48	64	60	56
$z_{u_{min}}$	0.1	0.0	0.1	0.1	0.0	0.1
u_{max} (m s^{-1})	13.3	10.0	9.8	9.4	2.4	7.2
$r_{u_{max}}$ (km)	28	36	40	56	48	48
$z_{u_{max}}$ (km)	1.1	1.1	1.1	1.7	3.0	2.0
V_{tmax} (m s^{-1})	79.5	83.1	66.5	54.3	62.5	58.4
$r_{V_{tmax}}$ (km)	35	30	50	60	65	60
$z_{V_{tmax}}$ (km)	0.6	0.7	0.6	0.7	1.2	0.8

the MRF scheme, have reached their mature stage. The extreme values of both quantities and their locations are summarized in Table II. A common feature of all six calculations is the shallow region of inflow that characterizes the boundary layer and a region of outflow that surmounts it at small radii. With the MRF and Gayno–Seaman schemes (panels (e) and (f)), the inflow is weaker than in the other schemes and much weaker in the case of the MRF scheme. The outflow maximum with the MRF scheme is not evident with the chosen contour interval. In all cases, the maximum tangential wind component occurs close to the top of the inflow layer. This feature was found by Zhang *et al.* (2001), Kepert and Wang (2001) and discussed in M3. Note that there are appreciable differences in the structure of both velocity components between different schemes. In particular, the depth and strength of the low-level inflow vary between them, as does the radius at which the maximum inflow occurs (see Table II). With the unmodified bulk scheme and the MRF scheme, the maximum inflow occurs at the surface, whereas in the other schemes it is slightly elevated at approximately 100 m.

The structural differences found above are similar to those noted by BT00, although they found that the Burk–Thompson scheme gave the strongest vortex with the maximum inflow, while the bulk scheme was marginally weaker in both respects (see their figures 9 and 10). BT00 showed fields throughout the whole troposphere, whereas we focus attention here on the lower troposphere below a height of 3 km. As in our study, BT00 found that the

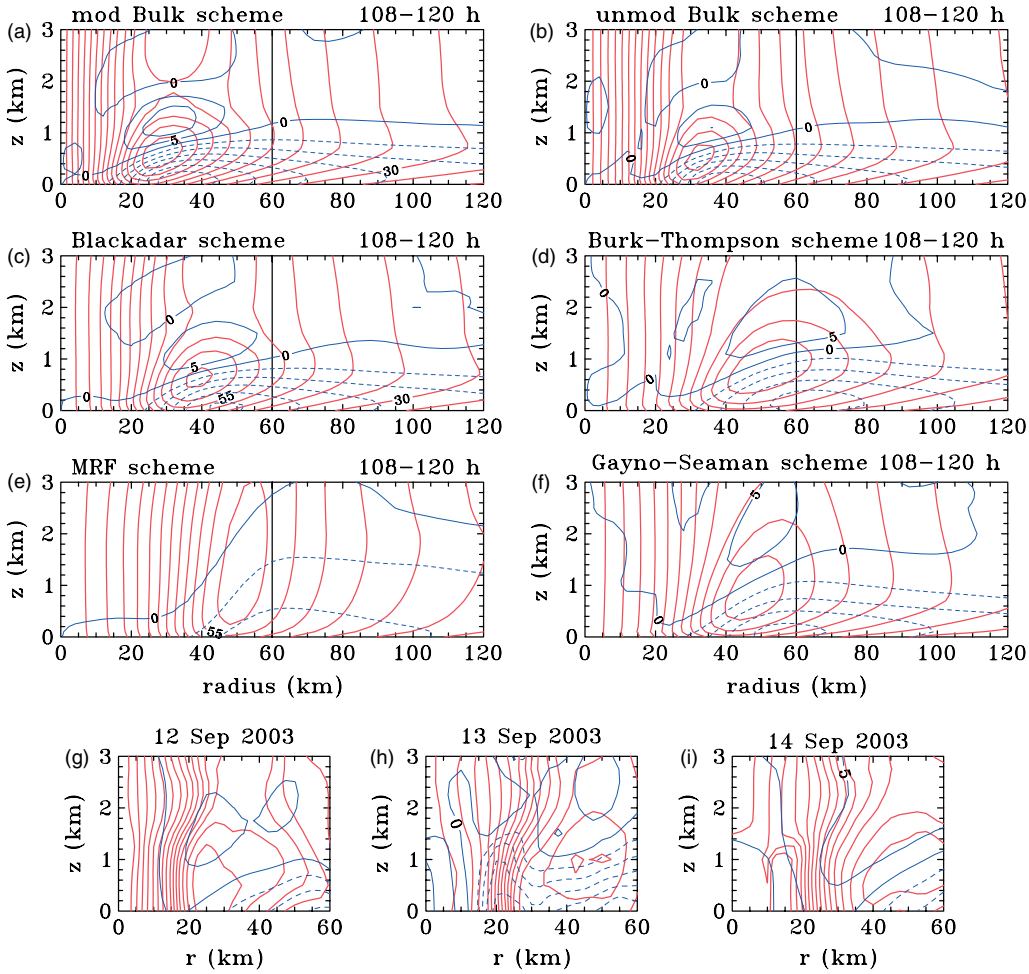

Figure 2. Radius–height cross-sections of azimuthally-averaged radial (thin/blue contours) and tangential wind-speed (thick/red contours) components in the lowest 3 km averaged at 15 minute intervals during the period 108–120 hours for the different boundary-layer schemes. (a) Modified bulk scheme, (b) unmodified bulk scheme, (c) Blackadar scheme, (d) Burk–Thompson scheme, (e) MRF scheme and (f) Gayno–Seaman scheme. Contour interval 5 m s^{-1}. The solid vertical line at 60 km radius delineates the region to be compared with panels (g)–(i), which show similar cross-sections from Bell and Montgomery's analyses of data obtained on three days during *Hurricane Isabel* (2003).

MRF scheme gave the deepest and weakest inflow and the weakest tangential wind maximum, and it is the only scheme not to show a low-level outflow maximum at the contour level plotted. It is interesting to note that the depth of the strong inflow layer, as judged by the $u = -5\,\mathrm{m\,s^{-1}}$ contour, increases inwards in all cases until a radius ranging from about 85 km for the MRF scheme to about 55 km for the unmodified bulk scheme. Thereafter the depth decreases as the radial flow declines towards the rotation axis. From Table II it is seen that the radius at which $v_{\max}$ occurs lies approximately 8 km inwards of the position of $u_{\min}$, except in the Burk–Thompson scheme, where it lies approximately 12 km inwards.

The strength, radius and height of the maximum radial outflow vary also. Time series of the maximum radial outflow below 3 km are shown in panel (d) of Figure 1. These time series are particularly noisy, a reflection of strong inertial wave activity in the region encompassing this maximum as suggested by animations of the radial velocity field. Note that, at all times, the outflow is weakest with the MRF scheme (max. values $\leq 5\,\mathrm{m\,s^{-1}}$) and strongest with the modified bulk scheme (max. values up to $17\,\mathrm{m\,s^{-1}}$). Again, these results are broadly in line with those of BT00 (see their figures 9 and 10).

3.3. *Comparison with observations*

Panels (g), (h) and (i) of Figure 2 show for comparison radius–height cross-sections of azimuthally averaged radial and tangential wind components in the lowest 3 km obtained from analyses of data collected during *Hurricane Isabel* (2003) (Bell and Montgomery, 2008). These data were obtained on three days (12–14 September) when Isabel was a Category 5 storm and therefore stronger than the vortices in panels (a)–(f). While there are significant differences in detail between the observations on each day, they do show a common feature between themselves and with our calculations, namely that the maximum tangential wind lies within the inflow layer or just on its boundary as noted earlier. Moreover, the inflow is surmounted by a layer of radial outflow. One striking feature of the observations on 13 September, not seen on other days, nor in any of the calculations, is that the maximum tangential wind lies well outside the inflow layer. At this stage we are unable to offer an explanation for this feature.

3.4. *Mature-stage total wind structure*

Hurricane forecasters are especially interested in the pattern of total wind speed and, in particular, how the near-surface

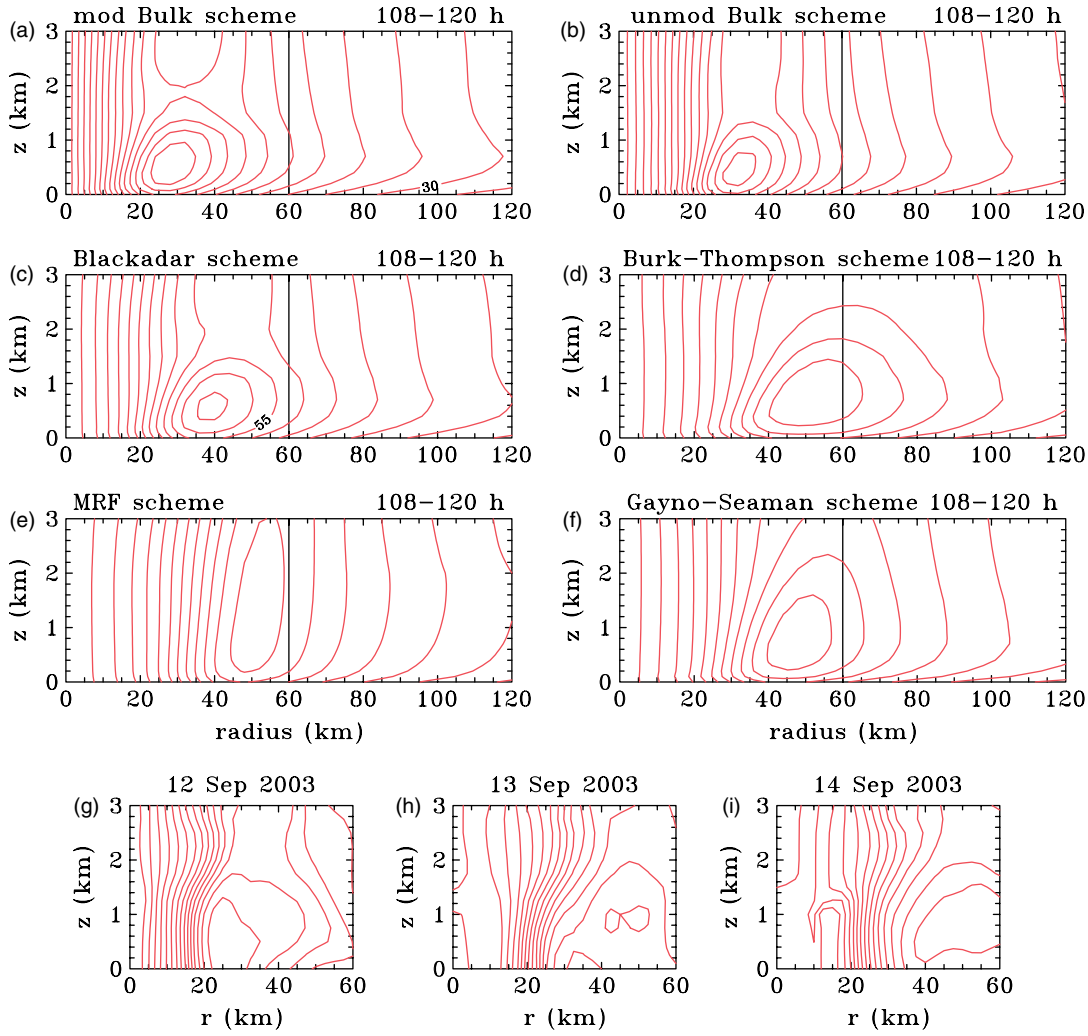

Figure 3. Radius–height cross-sections of azimuthally-averaged total wind speed in the lowest 3 km averaged at 15 minute intervals during the period 108–120 hours for the different boundary-layer schemes. (a) Modified bulk scheme, (b) unmodified bulk scheme, (c) Blackadar scheme, (d) Burk–Thompson scheme, (e) MRF scheme and (f) Gayno–Seaman scheme. Contour interval 5 m s^{-1}. The solid vertical line at 60 km radius delineates the region to be compared with panels (g)–(i), which show similar cross-sections from Bell and Montgomery's analyses of data obtained on three days during *Hurricane Isabel* (2003).

wind speed is related to that at flight level in aircraft reconnaissance flights into hurricanes (typically 700 mb). For this reason, we show in Figure 3 the isotachs of total wind corresponding to the wind components in Figure 2. The details of the maxima and their location are summarized also in Table II. The total wind has an elevated maximum (V_{tmax}) in all schemes and its strength, time-averaged over the period 108–120 hours, varies between 51 m s^{-1} for the MRF scheme and 71 m s^{-1} for the unmodified bulk scheme. The radius at which the maximum occurs ranges from 30 km for the modified bulk scheme to 60 km for the MRF scheme and the height at which it occurs ranges from 0.5 km for the unmodified bulk scheme to 1.2 km for the MRF scheme. It is seen in Figure 3 that a low-level wind-speed maximum occurs at all radii, except within a few tens of kilometres of the centre, depending on the scheme.

Panels (g), (h) and (i) of Figure 3 show similar radius–height cross-sections obtained from the *Hurricane Isabel* analyses. As in Figure 2, the comparison is limited by the difference in intensity, both between the observations themselves on different days and from the calculations. Nevertheless the observations and calculations are qualitatively similar and the observations show also an elevated maximum of total wind.

3.5. *Comparison with dropsonde soundings*

It is pertinent to compare vertical profiles of the total wind speed with those obtained by Franklin *et al.* (2003) from an analysis of Global Positioning System (GPS) dropsonde soundings in the inner core region of hurricanes. These authors constructed mean wind-speed profiles for eyewall dropsondes released within 5.6 km of the flight-level radius of maximum wind (RMW), for eyewall sondes released at least 7.4 km radially outward of the RMW, and for eyewall sondes released at least 7.4 km radially inward of the RMW (their figure 10). Their data provide a useful benchline check of the boundary-layer schemes examined here.

Figure 4 compares similar vertical profiles of mean wind obtained using the five boundary-layer schemes with those given in Franklin *et al.*'s figure 10. The profiles are taken at the radius of maximum total wind speed at a height of 2.9 km and expressed as a ratio of this wind-speed maximum. It is seen that the MRF curve comes closest to reproducing Franklin's RMW curve (labelled F1 in Figure 4), while

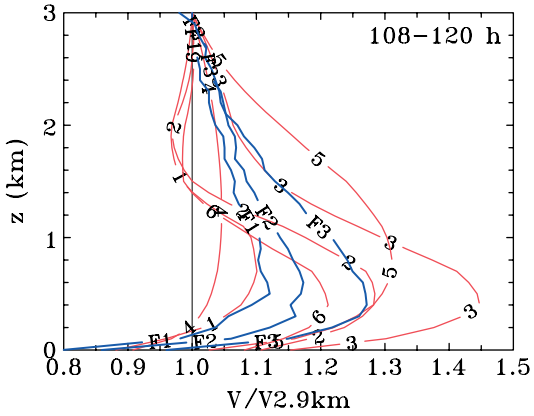

Figure 4. Vertical profiles of the ratio of azimuthal-mean total wind speed to that at 2.9 km at the radius of maximum tangential wind in the time-averaged fields from 108–120 h in the set of calculations with different boundary-layer parametrizations: 1 = bulk scheme, 2 = Blackadar scheme, 3 = Burk–Thompson scheme, 4 = MRF scheme, 5 = Gayno–Seaman scheme, 6 = unmodified bulk scheme. The three thick curves show the mean wind-speed profiles for eyewall dropsondes released within 5.6 km (3 nautical miles, hereafter n mi) of the flight-level RMW (labelled F1), those released at least 7.4 km (4 n mi) radially outward of the RMW (labelled F2) and those released at least 7.4 km (4 n mi) radially inward of the RMW (labelled F1), taken from Franklin *et al.* (2003). The Franklin sounding data are expressed as a fraction of the 700 mb (near $z = 2.9$ km) wind speed.

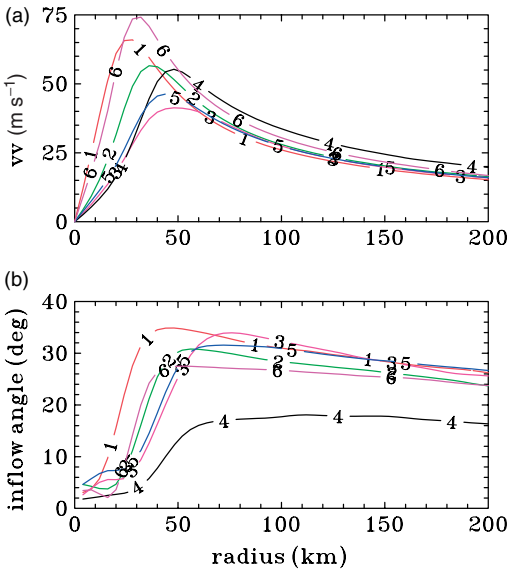

Figure 5. (a) Radial profiles of azimuthal-mean total surface wind speed for the period 108–120 hours in the six calculations: 1 = bulk scheme, 2 = Blackadar scheme, 3 = Burk Thompson scheme, 4 = MRF scheme, 5 = Gayno–Seaman scheme, 6 = unmodified bulk scheme. (b) Corresponding inflow angles $\tan^{-1}(u/v)$.

the Gayno–Seaman curve lies close to Franklin's F2 curve. The F2 curve refers to the sondes released outside of the flight-level RMW and F3 to those released inside. The Burk–Thompson curve is the outlier, having a maximum in excess of Franklin's F3 curve between 500 m and 1800 m and having the smallest values above about 2 km. Curves for the other schemes (the modified and unmodified bulk schemes and the Blackadar scheme) are within the observed range of variability below 1–1.5 km, but are generally smaller than the observed curves above 1.5 km. The unmodified bulk scheme gives values that are too large compared with the observed curves near the surface. All except this scheme have maxima that are somewhat higher than those in the observations. Nevertheless, most of the schemes have a maximum ratio that is comparable in magnitude with those observed. In all schemes except the unmodified bulk scheme, the ratio of near-surface winds to winds at 2.9 km lies within the range found in the observations. In making these comparisons, it should be kept in mind that there is a lot of variability in the observational data from which the mean profiles are constructed.

3.6. *Surface wind*

Perhaps the feature of most immediate interest to hurricane forecasters from an axisymmetric perspective would be the radial profile of near-surface wind. Figure 5 shows radial profiles of azimuthal-mean total surface wind speed, averaged during the period 108–120 hours, in the five calculations. It shows also the corresponding profiles of inflow angle $[\tan^{-1}(u/v)]$, where u and v are the radial and tangential velocity components. The strongest vortex at this time, as measured by the surface wind, is that with the unmodified bulk scheme, and the weakest is that with the Burk–Thompson scheme. The radius at which the maximum surface wind speed occurs varies from 27 km for the unmodified bulk scheme to 47 km for the MRF scheme. The maximum inflow angles for all except the MRF scheme lie in the range 27–35° and occur at radii between 40 and 70 km. The MRF scheme has the smallest angle of about 17°. Surface inflow angles derived from recent observational studies of *Hurricane Georges* (1998), *Hurricane Mitch* (1998), *Hurricane Danielle* (1998) and *Hurricane Isabel* (2003) show maximum inflow angles of 24, 18, 24 and 26°, respectively.** From these data one would conclude that all except the MRF scheme tend to overestimate the surface inflow angle to some degree.

Another relationship of interest to hurricane forecasters is that between the maximum surface wind speed (V_{tsmax}) and the maximum wind speed (V_{tfmax}) at the normal flight level of reconnaissance aircraft (about 3 km) (Powell *et al.*, 2009). In their observational study, Powell *et al.* found the typical ratio of these two wind maxima to be 0.83 with a standard deviation of 9%. The corresponding values for the six calculations in Figure 5 range from 0.7 for the bulk scheme to 1.07 for the unmodified bulk scheme. The average of all schemes is 0.90 with a standard deviation of 0.05. In all calculations, the radius of V_{tsmax} lies in a range 6–8 km *inside* that of V_{tfmax}, similar to the value found by Powell *et al.* (2009).

3.7. *Mature-stage vertical velocity*

Figure 6 shows radius–height cross-sections of azimuthal-mean vertical velocity averaged at 15 minute intervals for the 12 hour period 108–120 hours. With all schemes except the MRF scheme, there are two local maxima, one at a height of the order of 1–2 km and a second at a height of between 8 and 10 km as discussed in M3, although the lower maxima are not apparent for the unmodified bulk and Gayno–Seaman

**The first of these angles is based on the right panels of the first and third rows of figure 9 in Kepert (2006a), the second on panels (b) and (d) of figure 6 in Kepert (2006b), the third from the second panels of each column of figure 4 in Schwendike and Kepert (2008) and the fourth on the two right panels of figure 19 in the same article.

Table III. Maximum vertical velocity (w_{Lmax}, u_{Umax}) averaged during the period 108–120 hours together with the radii ($r_{w_{\mathrm{Lmax}}}$, $r_{u_{\mathrm{Umax}}}$) and heights ($z_{w_{\mathrm{Lmax}}}$, $z_{u_{\mathrm{Umax}}}$) at which they occur for the five boundary-layer schemes as indicated. Here 'L' and 'U' refer to isolated maximum vertical velocities below and above a height of 2.5 km, respectively.

Scheme	Mod bulk	Unmod bulk	Blackadar	Burk–Thompson	MRF	Gayno–Seaman
w_{Lmax} (m s^{-1})	1.8	1.5	1.2	1.1	–	1.3
$r_{w_{\mathrm{Lmax}}}$ (km)	24	32	36	48	–	48
$z_{w_{\mathrm{Lmax}}}$ (km)	0.8	0.9	1.0	1.2	–	1.8
u_{Umax} (m s^{-1})	2.2	2.3	1.5	1.2	2.1	1.2
$r_{u_{\mathrm{Umax}}}$ (km)	36	40	48	72	56	64
$z_{u_{\mathrm{Umax}}}$ (km)	8.9	8.7	8.8	8.3	7.4	6.0

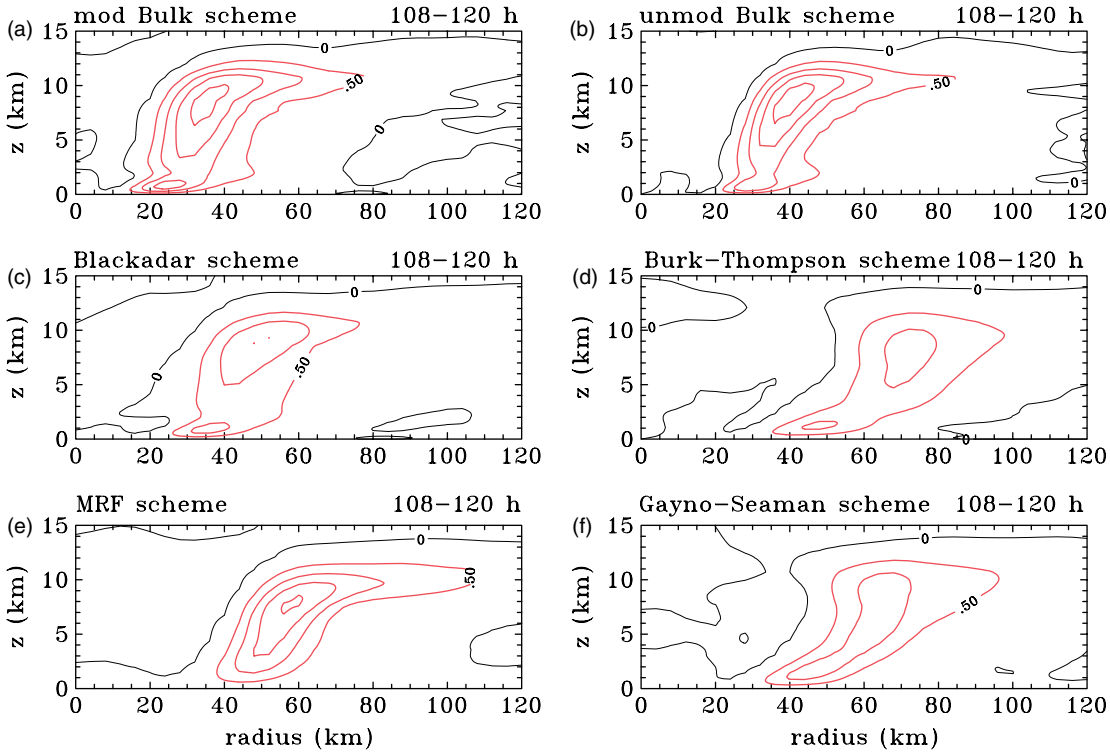

Figure 6. Radius–height cross-sections of azimuthally-averaged vertical velocity averaged at 15 minute intervals during the period 108–120 hours for the different boundary-layer schemes. (a) Unmodified bulk scheme, (b) modified bulk scheme, (c) Blackadar scheme, (d) Burk–Thompson scheme, (e) MRF scheme and (f) Gayno–Seaman scheme. Contour interval 0.5 m s^{-1}. Zero contours are thin black. The isolated maximum below 2.5 km indicated in Table III for the Gayno–Seaman scheme is not seen in panel (f) with the chosen contour interval.

schemes with the contour interval chosen in the figure. The strength and location of these maxima are summarized in Table III. As for the other fields, there are considerable differences in the strength of the maxima and the radii and heights at which they occur between the different schemes. The lower maximum ranges in strength between 1.0 m s^{-1} and 2.0 m s^{-1}, its radius between 20 and 36 km and its height between 0.8 km and 1.1 km. The upper maximum ranges in strength between 1.3 and 2.0 m s^{-1}, its radius ranges between 36 and 56 km and its height ranges between 8.1 km and 9.6 km. Again these differences are broadly similar to those found by BT00, as can be seen by comparing panels (a), (b), (c) and (e) of Figure 6 with panels (b), (c), (a) and (d) of figure 8 in BT00, respectively. In their case the maximum vertical velocities range from 0.75+ m s^{-1} in the MRF scheme to 1.35+ m s^{-1} in the Burk–Thompson scheme (these data are estimated from their contour plots and the values slightly exceed the highest contour, hence the '+' sign).

3.8. *Mature-stage agradient winds*

An important feature of the boundary layer is the net inward force that develops at low levels outside the eyewall region as a result of friction. There the tangential flow is subgradient and this force drives the strong inflow that is now recognized as being important for the spin-up of the inner core as discussed in M3. The net (agradient) radial force, $-(1/\rho)(\partial p/\partial r) + v^2/r + fv$, is related to the agradient wind, v_{a}, defined as the azimuthal-mean tangential wind minus the gradient wind, v_{g}, which is the positive solution of the gradient wind equation $v_{\mathrm{g}}^2/r + fv_{\mathrm{g}} - (1/\rho)(\partial p/\partial r) = 0$. Fields of v_{a} show regions in which the flow deviates from gradient-wind balance. Because of the importance of the agradient flow in the inner-core region of a tropical cyclone, we show in Figure 7 radius–height cross-sections of v_{a}, averaged at 15 minute intervals for the period 108–120 hours for the different boundary-layer schemes. Again there are marked differences in v_{a} between the schemes. These

differences are consistent with other flow features, such as the strength of the inflow maximum and that of the overlying outflow maximum inside the inner-core updraught.

The weakest subgradient flow ($v_a < 0$) occurs with the MRF scheme while all schemes show considerable supergradient flow ($v_a > 0$) in the inner core region. The maximum supergradient flow in the six calculations ranges between 10.5 m s^{-1} for the Blackadar scheme and 19.4 m s^{-1} for the modified bulk scheme. The average value for all six schemes is 15.8 m s^{-1} with a standard deviation of 1.2 m s^{-1}. This is a little higher than the observed values found by Schwendike and Kepert (2008), which are of the order of 10 m s^{-1}, or about 12% of the gradient wind at 600 m. The radius of the maximum v_a ranges between 16 km for the Blackadar scheme and 48 km for the Burk–Thompson scheme and its height ranges from 200 m for the Blackadar scheme to 1 km for the Gayno–Seaman scheme and over 3 km for the MRF scheme.

The maximum magnitude of negative v_a ranges between 8.3 m s^{-1} for the MRF scheme and 19.0 m s^{-1} for the modified bulk scheme. The average value for all six schemes is 13.7 m s^{-1} with a standard deviation of 1.3 m s^{-1}. The average radius of the minimum v_a is 60 km with a standard deviation of 4.8 km and the height of the minimum occurs at the surface in all schemes.

3.9. *Eddy diffusivity*

While the boundary-layer schemes investigated have various degrees of sophistication, almost all seek to determine some local value of turbulent diffusivity, $K(r,z)$, to close the momentum and thermodynamic equations, the exception being the Blackadar scheme, which uses a non-local mixing algorithm in the convective regime. In some schemes, the determination of K is based on empirical formulae, while in others it is based on a calculation of the turbulent kinetic energy, which may be carried as a prognostic quantity (e.g. in the Burk–Thompson and Gayno–Seaman schemes). BT00 showed vertical cross-sections of azimuthally-averaged eddy diffusivity for the four schemes that they studied. We performed similar calculations and found similar distributions. Examples of these are shown in Figure 8 for the modified bulk scheme and MRF scheme where, as for the fields shown earlier, the values are time-averaged over the period 108–120 hours. The patterns in all[††] five schemes are similar, showing a low-level maximum of diffusivity in the region of maximum tangential wind speed as well as elevated values in the eyewall updraft, which is indicated by the 0.2 m s^{-1} contour of vertical velocity in the figure. They show also strong radial and vertical gradients of K.

Maximum values of K for the various schemes are shown as time series in Figure 9, where it is seen that the MRF scheme is by far the most diffusive with a maximum of nearly 600 m^2 s^{-1}, the Gayno–Seaman scheme is relatively diffusive with a maximum of about 250 m^2 s^{-1}, and the other schemes are comparable with maximum diffusivities in the range 60–100 m^2 s^{-1}. As noted by BT00, the high diffusivity in the MRF scheme would account for the comparatively weak inflow and upflow in the MRF scheme, but it does not explain why, with this scheme, the vortex in our calculation is still intensifying at 5 days.

The only observed estimates for K that we are aware of are those determined from flight-level wind measurements at an altitude of about 500 m in *Hurricanes Allen* (1980) and *Hugo* (1989). In *Hugo* these were about 110 m^2 s^{-1} beneath the eyewall, where the near-surface wind speeds were about 60 m s^{-1}, and in *Allen* they were up to 74 m^2 s^{-1}, where wind speeds were about 72 m s^{-1} (Zhang *et al.*, 2010). One might be tempted to judge that the MRF and Gayno–Seaman schemes are much too diffusive, whereas the other schemes have broadly realistic diffusivities. However, it would be premature to draw firm conclusions from such a limited comparison!

The boundary-layer scale analysis of Vogl and Smith (2009) shows that the boundary-layer depth scales as $\sqrt{2K/I}$, where I is the inertial stability parameter. Since both K and I have strong radial gradients, it is of interest to see how this scale varies with both radius and height. We show in Figure 10 the variation of this scale for the modified bulk scheme, one of the least diffusive schemes, and for the MRF scheme, the most diffusive. For the bulk scheme, at any given height below about 1 km, this scale slowly increases with decreasing radius outside of the eyewall updraught (as defined above), reaching a maximum within the upflow and decreasing sharply on the inner edge of the updraught. *It does not decrease with decreasing radius as the eyewall is approached, as is be suggested by a scale analysis with constant diffusivity* (Vogl and Smith, *op cit.*). The contours for the MRF scheme show a larger increase with decreasing radius outside the eyewall updraught, an elevated maximum and values that are generally much larger than for the bulk scheme. In both cases there is a sharp decline in the scale towards the inner edge of the updraught, but the applicability of boundary-layer scaling in this region is questionable (Smith and Montgomery, 2010).

3.10. *Turbulent kinetic energy*

Retrievals of turbulent kinetic energy (TKE) from Doppler radar data in hurricanes suggest that boundary-layer turbulence is being lifted into the eyewall clouds to supplement the turbulence generated locally within the eyewall itself (Lorsolo *et al.*, 2009). Thus it is of interest to examine the structure of TKE for the Burk–Thompson and Gayno–Seaman schemes, which carry this quantity as a prognostic variable. We calculated radius–height cross-sections of azimuthally-averaged TKE for these schemes averaged over the period 108–120 hours. The patterns are very similar to those of eddy diffusivity in Figure 8 and are not shown. In particular, they have a low-level maximum in the region of maximum tangential wind speed as well as elevated values in the eyewall updraft. The maximum values at 120 h are about 24 m^2 s^{-2} with the Burk–Thompson scheme and 14 m^2 s^{-2} with the Gayno–Seaman scheme, comparable with those reported by Lorsolo *et al.* (2009) (15 m^2 s^{-2}) and Zhang *et al.* (2010) (25 m^2 s^{-2}).

4. Discussion and interpretation

We have shown that there are significant differences in the time evolution and low-level structure of vortices in the simulations with different representations of the boundary layer. While there is no complete theory for the mature

[††]The non-local mixing algorithm in the Blackadar scheme is not invoked within 200 km of the axis.

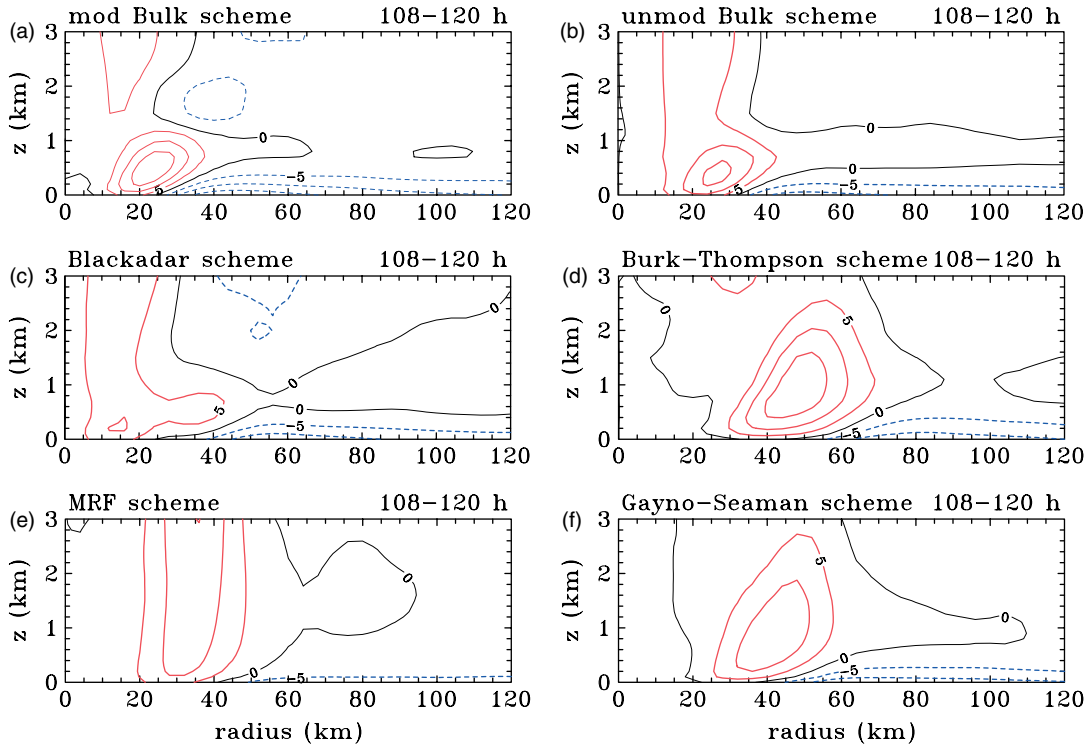

Figure 7. Radius–height cross-sections of azimuthally-averaged agradient wind during the period 108–120 hours for the different boundary-layer schemes. (a) Modified bulk scheme, (b) unmodified bulk scheme, (c) Blackadar scheme, (d) Burk–Thompson scheme, (e) MRF scheme and (f) Gayno–Seaman scheme. Contour interval 5.0 m s^{-1}. Zero contours are thin black, negative contours dashed.

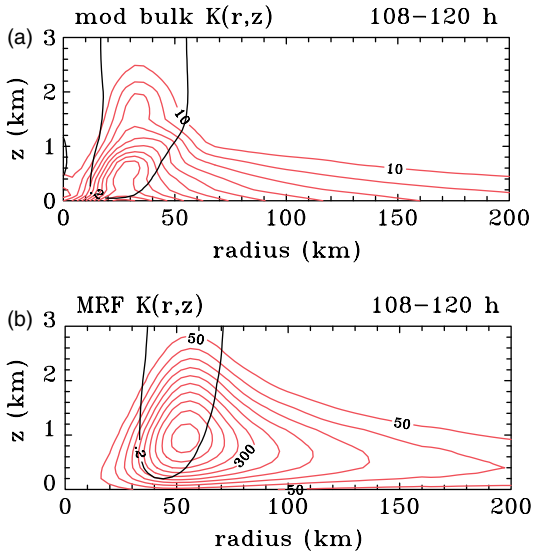

Figure 8. Radius–height cross-section of azimuthally-averaged eddy diffusivity during the period 108–120 hours, for (a) the unmodified bulk scheme (contour interval 10 m^{2}s^{-1}) and (b) the MRF scheme (contour interval 50 m^{2}s^{-1}). The thick black contours show the 0.2 m s^{-1} contour of azimuthally averaged vertical velocity.

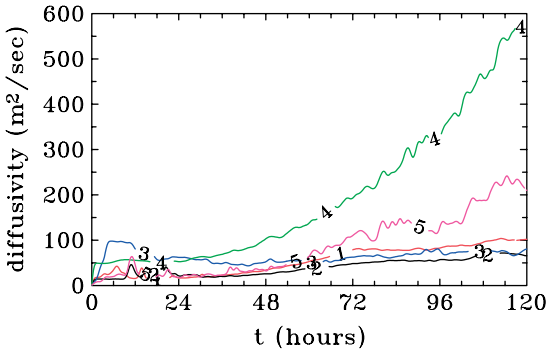

Figure 9. Time series of maximum azimuthally-averaged eddy diffusivity for the five modified boundary-layer schemes: 1 = bulk scheme, 2 = Blackadar scheme, 3 = Burk–Thompson scheme, 4 = MRF scheme, 5 = Gayno–Seaman scheme.

tropical cyclone with which to interpret these differences fully, it is possible to relate certain aspects of the boundary-layer structure to the differences in intensity. In doing this it needs to be kept in mind that we are comparing six deterministic calculations when it is known from the work of Nguyen *et al.* (2008) and Shin and Smith (2008) that, because of the intrinsically stochastic nature of deep convection, small differences between individual calculations may not be significant.

The boundary-layer scale analysis of Vogl and Smith (2009) shows that the boundary-layer depth is proportional to the square root of the eddy diffusivity, so that large diffusivities lead to deep inflow layers. Calculations using the slab boundary-layer model of Smith and Vogl (2008) indicate that the effective frictional stress within the boundary layer increases with decreasing boundary-layer depth, because then the surface stress is spread over a shallower layer. The calculations show also that a larger effective stress leads to a larger disruption of gradient-wind balance and hence to stronger inflow in the boundary layer. In turn, stronger inflow brings air parcels to small radii rapidly, minimizing the loss of absolute angular momentum on account of the frictional torque, even though the torque itself is increased. While the slab model cannot be expected to be an accurate representation of a full boundary layer for reasons articulated in Smith and Vogl *op. cit.*, the results

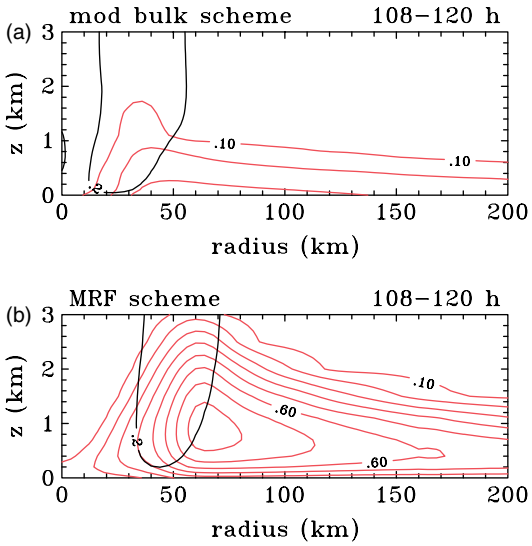

Figure 10. Radius–height cross-section of azimuthally-averaged boundary-layer depth scale during the period 108–120 hours, for (a) the modified bulk scheme and (b) the MRF scheme, contour interval 0.1 km. The thick (black) contour shows the 0.2 m s^{-1} contour of azimuthally averaged vertical velocity.

described herein are broadly consistent with the forgoing interpretation that the schemes with deeper inflow layers have weaker inflow.

The five modified schemes can be divided into three groups: the bulk and Blackadar schemes, which have relatively shallow inflow layers about 800–850 m deep; the Burk–Thompson and Gayno–Seaman schemes, which have intermediate inflow depths of about 1 km; and the MRF scheme, where the inflow depth is about 1.5 km. Here we use the maximum depth of the -5 m s^{-1} contour as a measure of the boundary layer depth. Referring to Table II, we note that the bulk and Blackadar schemes have the largest inflow speeds (33.5 and 25.8 m s^{-1}, respectively), the largest tangential wind speeds (79.4 and 66.4 m s^{-1}) and the smallest RMWs (28 and 40 km). The Burk–Thompson and Gayno–Seaman schemes have more moderate inflow speeds (22.5 and 22.0 m s^{-1}), more moderate tangential wind speeds (54.2 and 58.2 m s^{-1}) and larger RMWs (52 and 58 km). Finally, the MRF scheme has the weakest inflow speed, 13.8 m s^{-1}, the deepest inflow (about 1.5 km), but, surprisingly, not the weakest tangential wind speed (62.4 m s^{-1}), although the RMW is large: 52 km. Further, it is the only scheme for which the vortex has not reached a quasi-steady state after five days of integration. It is beyond the scope of this article to delve into this discrepancy further, but it should be noted that, on account of the extreme and possibly unrealistically high diffusivities, the boundary layer in this scheme does not depart far from gradient balance compared with the other schemes (see Figure 7). We are working to analyse this discrepancy in more detail: it is possible, for example, that the continued strengthening is associated with a larger diabatic forcing, which we have still to quantify.

It is probable that the relatively small differences between the modified and unmodified bulk and Gayno–Seaman schemes can be attributed to the differences in the surface-exchange coefficients as argued by Hill and Lackman (2009), but the precise reasons require further study also. At present, the only theory we know of providing a relationship between the surface-exchange coefficients for enthalpy[‡‡] and momentum and the vortex intensity is that of Emanuel (1986), who developed a steady-state axisymmetric hurricane model in which the maximum swirling wind is proportional to the square root of the ratio of these exchange coefficients. In this theory, both exchange coefficients are assumed to have the same wind-speed dependence and the entire flow, *including the boundary layer*, is assumed to be in gradient-wind balance. None of these assumptions apply in the present calculations, so that the application of Emanuel's theory would seem questionable. Indeed, it has been shown recently that, at least for the bulk scheme, which is a relatively weakly diffusive scheme, and when the exchange coefficients are held constant, there is a regime in which the vortex intensification rate and intensity after four days of integration *increase (sic)* with increasing drag coefficient (Montgomery *et al.*, 2010). In this regime, the increased inflow with increasing drag coefficient is apparently sufficient to bring air parcels to smaller radii without them losing a commensurate amount of absolute angular momentum. This result is counter to the prediction of Emanuel's theory.

So far we have been able to show that doubling the drag coefficient in the calculations with the more diffusive schemes described above leads to stronger inflow, but weaker maximum tangential wind speeds. There is stronger inflow as well with the less diffusive bulk and Blackadar schemes, but with these schemes the maximum tangential wind speeds do not differ appreciably or systematically during most of the five days of integration.

There is no theory as yet that would enable us to relate the differences in drag to the differences in the forcing as characterized, say, by the radial gradient of the azimuthally-averaged diabatic heating rate (see for example Bui *et al.*, 2009). We would surmise that the heating rate is intimately related to the thermodynamic structure of the boundary layer, which will be the topic of a further article. Certainly, further research into the relationship between the thermodynamic structure of the boundary layer and the distribution of diabatic heating rate is required.

5. Conclusions

We have investigated the structure of the boundary layer in an idealized numerical model of a tropical cyclone. The study is motivated by recent findings highlighting the important dynamical role of the boundary layer to tropical-cyclone intensification. The calculations were carried out using the MM5 model. Predictions using one of five of the available schemes were compared, not only between themselves, but where possible with recent observational analyses of boundary-layer structure.

We have shown that there is a significant sensitivity of vortex evolution, including the rate of intensification and the low-level wind structure in the inner core region, to the particular boundary-layer scheme used. Some of these differences can be traced to the different eddy diffusivities determined by the schemes. The MRF scheme appears to be particularly overdiffusive compared with the others and with the only available observational estimates.

[‡‡] If the transfer coefficients for sensible and latent heat are the same, then the total heat transfer is equivalent to the transfer of moist enthalpy (Emanuel, 1995).

Further work is required to relate the diabatic forcing of vortices to the thermodynamical structure of the boundary layer for the various boundary-layer schemes.

The study falls short of being able to advocate the use of a particular scheme, although certain shortcomings of individual schemes are identified in relation to their ability to capture realistic vertical wind profiles and surface inflow angles. *We argue that the current inability to determine 'the optimum scheme' has implications for the predictability of tropical-cyclone intensification*. Our study and that of Braun and Tao (2000) provide an estimate of forecast uncertainty that follows from the uncertainty in knowing the optimum boundary-layer scheme to use.

This article has sought to elevate awareness of an important problem in the design of deterministic forecast models for hurricane intensity, namely the question of which boundary-layer scheme is most appropriate. Clearly a strategy needs to be developed to answer this question. Studies like those of Braun and Tao (2000) and Nolan *et al.* discussed earlier are unlikely to be able to determine the 'best scheme' by comparing model simulations with observations for the simple reason that other aspects of the model such as the representation of cloud microphysics have inherent uncertainties as well. In this regard, diagnostic studies of the type described by Kepert and coworkers that specifically focus on the boundary-layer structure might be more suited to providing an answer to the foregoing problem. However, such studies should be extended to consider different schemes and issues concerning the appropriate upper boundary condition to use where the air is ascending out of the boundary layer need to be resolved (Smith and Montgomery, 2010).

Acknowledgements

This research was supported by a grant from the German Research Council (Deutsche Forschungsgemeinschaft). We have benefited from many discussions about the boundary layer with Michael Montgomery and are grateful to him for his perceptive comments on the present manuscript. We are most grateful also to Saurabh Barve and Sang Nguyen for their expert help in tracking down a subtle coding error in our implementation of the bulk scheme in MM5, to Sang Nguyen for his comments on the appendix and to Michael Bell for kindly providing the data for the last panels of Figures 2 and 3.

A. Appendix: The boundary-layer schemes

A.1. The bulk scheme

The bulk scheme calculates the surface fluxes of sensible heat, latent heat and momentum by bulk-aerodynamic formulae. The fluxes between the individual model layers above the first model level are then calculated by a first-order (local K-mixing) scheme. The original parametrization calculates the bulk Richardson number to distinguish between a stable and an unstable case. The calculation of the surface-exchange coefficients then depends on the stability of the boundary layer. In our modification of the scheme, there is no distinction between a stable and an unstable boundary layer. In the unmodified version, the exchange coefficients are given by $C_u = [C_{uN}^{-1} - 25\exp(0.26\zeta - 0.030\zeta^{-2})]^{-1}$, $C_E = (C_{\theta N}^{-1} + C_u^{-1} - C_{uN}^{-1})^{-1}$ in the *unstable case* ($Ri_B < 0$) where $\zeta = \log_{10}(-Ri_B) - 3.5$, and $C_u = C_{uN}(1 - Ri_B/Ri_c)$, $C_E = C_{\theta N}(1 - Ri_B/Ri_c)$ in the *stable case* ($0 \le Ri_B \le 0.9Ri_c$). In both cases, $C_{uN} = [k^{-1}\log\{0.025(\overline{h} - \overline{z_s})/z_0\} + 8.4]z^{-1}$, $C_{\theta N} = (k^{-1}R\log\{0.025(\overline{h} - \overline{z_s})/z_0\} + 7.3)^{-1}$, with the critical bulk Richardson number given by $Ri_c = 3.05$. The constant $k = 0.35$ is the Kármán constant, the constant $R = 0.74$ is used in the surface-layer temperature profile function, z_0 is the roughness length, $\overline{h}$ is a horizontal average of the planetary boundary-layer height above mean sea level, $\overline{z_s}$ is a horizontal average of the surface height above mean sea level and Ri_B is the bulk Richardson number (Deardorff, 1972).

A.2. The Blackadar scheme

The version of the Blackadar scheme used here is that described by Zhang and Anthes (1982). It has two modules: one for the daytime convective state and one for the night-time stable state. Which module is invoked depends on the vertical temperature gradient in the lowest model layer and on the magnitude of $|z_h/L|$, where z_h is the height of the mixed layer and L is the Monin–Obukhov length. The vertical temperature gradient in the lowest model layer is characterized by the bulk Richardson number Ri_b. In the nocturnal module, the atmosphere is assumed to be stably stratified, or at most slightly unstable, and a first-order closure scheme is used. A 10 m depth surface layer, based on Monin–Obukhov similarity theory, is used. The nocturnal module is subdivided into three stability states. The night-time stable state is assumed when $Ri_b \ge 0.2$, the damped mechanical turbulent state when $0 < Ri_b < 0.2$ and the forced convection state when $Ri_b \le 0$ and $|z_h/L| \le 1.5$. The daytime module allows for free convection and is active when $Ri_b \le 0$ and $|z_h/L| \ge 1.5$. Discrete matrix forms of non-local theory are then used to parametrize convective circulations. In this theory, the vertical transfer of momentum, heat and moisture is not determined by the local mean gradient, but by the thermal structure of the whole mixed layer. The Blackadar scheme is the only one of those studied that applies non-local mixing in any of the stability states.

A.3. The Mellor–Yamada-based schemes

Both Mellor–Yamada-based schemes described here use a one-and-a-half order closure, which refers to level 2.5 in the Mellor–Yamada hierarchy (Mellor and Yamada, 1974). A comprehensive summary of the different closures is given by Stull (1988). In a one-and-a-half order closure, the eddy-exchange coefficient of an adiabatically-conserved quantity is related to the predicted TKE. This kind of scheme is often referred to as a 'TKE scheme'.

A.3.1. The Burk–Thompson scheme

The Burk–Thompson scheme was originally designed for the marine boundary layer (Burk and Thompson, 1982) and incorporated both level 2.5 and 3.0 schemes. The early versions of the scheme, which were implemented in the US Navy's Navy Operational Regional Atmospheric Prediction System (NORAPS), apply a higher vertical resolution than that in the model and include a counter-gradient flux term for temperature. These two features are not implemented in MM5 and only the level 2.5 version is available. The Louis

(1979) scheme is used to parametrize the surface layer and applies an empirical fit to the Businger profile functions. Horizontal advection, diffusion or vertical advection of TKE are not included.

A.3.2. The Gayno–Seaman scheme

The Gayno–Seaman scheme is a level-2.5 Mellor–Yamada-based scheme. In order to represent cloud water in a consistent way, the model uses liquid water potential temperature, θ_L, and total water mixing ratio, q_T, which are both conserved thermodynamic variables in non-precipitating clouds (Betts, 1973). The turbulent vertical transport of θ_L is parametrized using a counter-gradient heat flux term, based on the sensible heat flux, the boundary-layer height and the convective vertical velocity scale (Therry and Lacarrere, 1983). The Gayno–Seaman scheme is the only one in MM5 for which TKE is treated as a prognostic quantity and is advected both horizontally and vertically. The surface fluxes for the Gayno–Seaman scheme are based on the same Monin–Obukhov similarity parametrization used with the Blackadar scheme and the stability states are determined using the same criteria (Shafran *et al.*, 2000). In the unmodified version of the scheme, the momentum-exchange coefficient is given by $C_u = k(\theta_e - \theta)/(GZ10Z0 - \psi_H)$, where $GZ10Z0 = \log(\max(z, 10)/z_0)$ and z_0 is the roughness length. The enthalpy exchange coefficient, C_E, is zero under night-time stable conditions and conditions of damped mechanical turbulence. It has the value $-Ri_B h/z$ under conditions of forced convection and $-h/L$ under conditions of free convection. Here L is the Monin–Obukhov length, z is the height above the surface, h is the height of the planetary boundary layer, Ri_B is the bulk Richardson number, θ is the potential temperature, θ_e is the pseudo-equivalent potential temperature, ψ_H is a similarity function and again k is the Kármán constant.

A.4. The MRF scheme

The MRF scheme was developed initially for the United States National Centers for Environmental Prediction (NCEP) Medium-Range Forecast system by Hong and Pan (1996) and was implemented in MM5 by Dudhia and Hong, as stated in the corresponding piece of code. This scheme applies non-local K-mixing for potential temperature and water-vapour mixing ratio in the mixed layer, moist vertical diffusion in clouds and local K-mixing above clouds. The non-local mixing is implemented following a non-local diffusion concept by Troen and Mahrt (1986). The use of the term 'non-local' in this scheme is misleading as it refers to the flux of a particular quantity between adjacent layers calculated by applying a correction term for the local gradient. This correction term incorporates the contribution of the large-scale eddies to the total flux. The eddy-exchange coefficients, K, are calculated from a prescribed profile function of boundary-layer heights and scale parameters. The surface fluxes are calculated in the same way as in the Blackadar scheme.

The four boundary-layer stability states are determined using only the bulk Richardson number. In the night-time stable state ($Ri_b \geq 0.2$), all scaling parameters at the surface and all turbulent fluxes are set equal to zero. In the nocturnal damped mechanical turbulent state ($0 < Ri_b < 0.2$) the scaling parameters are determined by Ri_b and L (the Monin–Obukhov length). In the nocturnal, forced-convection state ($Ri_b = 0$), the scaling parameters are determined by the local Richardson number Ri only (local K theory). When $Ri_b < 0$, the daytime module is used and the counter-gradient terms take effect.

References

Anthes RA, Chang SW. 1978. Response of the hurricane boundary layer to changes of sea-surface temperature in a numerical model. *J. Atmos. Sci.* **35**: 1240–1255.

Bell MM, Montgomery MT. 2008. Observed structure, evolution, and potential intensity of Category 5 *Hurricane Isabel* (2003) from 12 to 14 September. *Mon. Weather Rev.* **65**: 2025–2046.

Betts AK. 1973. Non-precipitating cumulus convection and its parameterization. *Q. J. R. Meteorol. Soc.* **99**: 178–196.

Black PG, D'Asoro EA, Drennan WM, French JR, Niller PP, Sanford TB, Terril EJ, Walsh EJ, Zhang JA. 2007. Air–sea exchange in hurricanes. Synthesis of observations from the coupled boundary-layer air–sea transfer experiment. *Bull. Am. Meteorol. Soc.* **88**: 357–374.

Blackadar AK. 1976. 'Modelling the nocturnal boundary layer'. In *Third Symp. on Atmospheric Turbulence, Diffusion and Air Quality*. American Meteorological Society: Raleigh; pp 46–49.

Blackadar AK. 1978. 'Modelling pollutant transfer during daytime convection'. In *Fourth Symp. on Atmospheric Turbulence, Diffusion and Air Quality*. American Meteorological Society: Reno; pp 443–447.

Blackadar AK. 1979. High resolution models of the planetary boundary layer. *Advances in Environmental Science and Engineering*. 50–52.

Braun SA, Tao W-K. 2000. Sensitivity of high-resolution simulations of *Hurricane Bob* (1991) to planetary boundary-layer parameterizations. *Mon. Weather Rev.* **128**: 3941–3961.

Bui HB, Smith RK, Montgomery MT, Peng J. 2009. Balanced and unbalanced aspects of tropical-cyclone intensification. *Q. J. R. Meteorol. Soc.* **135**: 1715–1731.

Burk SD, Thompson WT. 1982. Operational evolution of a turbulence closure model forecast system. *Mon. Weather Rev.* **110**: 1535–1543.

Davis CA and co-authors. 2008. Prediction of landfalling hurricanes with the advanced hurricane WRF model. *Mon. Weather Rev.* **136**: 1990–2005.

Deardorff JW. 1972. Parameterization of the planetary boundary layer for use in general circulation models. *Mon. Weather Rev.* **100**: 93–106.

Dudhia J. 1993. A non-hydrostatic version of the Penn State–NCAR mesoscale model: Validation tests and simulation of an Atlantic cyclone and cold front. *Mon. Weather Rev.* **121**: 1493–1513.

Emanuel KA. 1986. An air–sea interaction theory for tropical cyclones. Part I: Steady state maintenance. *J. Atmos. Sci.* **43**: 585–604.

Emanuel KA. 1995. Sensitivity of tropical cyclones to surface exchange coefficients and a revised steady-state model incorporating eye dynamics. *J. Atmos. Sci.* **52**: 3969–3976.

Emanuel KA. 1997. Some aspects of hurricane inner-core dynamics and energetics. *J. Atmos. Sci.* **54**: 1014–1026.

Franklin JL, Black ML, Valde K. 2003. GPS dropwindsonde wind profiles in hurricanes and their operational implications. *Weather Forecasting* **18**: 32–44.

Grell GA, Dudhia J, Stauffer DR. 1995. '*A description of the fifth generation Penn State/NCAR mesoscale model (MM5)*', NCAR Technical Note NCAR/TN-398+STR, 138 pp.

Hill KA, Lackmann GM. 2009. Analysis of idealized tropical cyclone simulations using the Weather Research and Forecasting model: sensitivity to turbulence parameterization and grid spacing. *Mon. Weather Rev.* **137**: 745–765.

Hong S-Y, Pan H-L. 1996. Nonlocal boundary layer vertical diffusion in a medium-range forecast model. *Mon. Weather Rev.* **124**: 2322–2339.

Janjić ZI. 1990. The step-mountain coordinate: Physical package. *Mon. Weather Rev.* **118**: 1429–1443.

Janjić ZI. 1994. The step-mountain eta coordinate model: Further developments of convection, viscous sublayer, and turbulence closure schemes. *Mon. Weather Rev.* **122**: 927–945.

Jordan CL. 1958. Mean soundings for the West Indies area. *J. Meteorol.* **15**: 91–97.

Kepert JD. 2001. The dynamics of boundary layer jets within the tropical cyclone core. Part I: Linear Theory. *J. Atmos. Sci.* **58**: 2469–2484.

Kepert JD. 2006a. Observed boundary-layer wind structure and balance in the hurricane core. Part I. *Hurricane Georges*. *J. Atmos. Sci.* **63**: 2169–2193.

Kepert JD. 2006b. Observed boundary-layer wind structure and balance in the hurricane core. Part II. *Hurricane Mitch*. *J. Atmos. Sci.* **63**: 2194–2211.

Kepert JD, Wang Y. 2001. The dynamics of boundary layer jets within the tropical cyclone core. Part II: Nonlinear enhancement. *J. Atmos. Sci.* **58**: 2485–2501.
Lorsolo S, Zhang JA, Marks F, Gamache J. 2009. Estimation and mapping of hurricane turbulent energy using airborne Doppler measurements. *Mon. Weather Rev.* **138**: 3656–3670.
Louis JF. 1979. A parametric model of vertical eddy fluxes in the atmosphere. *Boundary-Layer Meteorol.* **17**: 187–202.
Mellor GL, Yamada T. 1974. A hierarchy of turbulence closure models for planetary boundary layers. *J. Atmos. Sci.* **31**: 1791–1806.
Montgomery MT, Nguyen SV, Smith RK. 2008. Do tropical cyclones intensify by WISHE? *Q. J. R. Meteorol. Soc.* **135**: 1697–1714.
Montgomery MT, Smith RK, Nguyen SV. 2010. Sensitivity of tropical cyclone models to the surface exchange coefficients. *Q. J. R. Meteorol. Soc.* In press.
Nguyen CM, Smith RK, Zhu H, Ulrich W. 2002. A minimal axisymmetric hurricane model. *Q. J. R. Meteorol. Soc.* **128**: 2641–2661.
Nguyen SV, Smith RK, Montgomery MT. 2008. Tropical-cyclone intensification and predictability in three dimensions. *Q. J. R. Meteorol. Soc.* **134**: 563–582. (M1).
Nolan DS, Zhang JA, Stern DP. 2009a. Evaluation of planetary boundary layer parameterizations in tropical cyclones by comparison of in-situ observations and high-resolution simulations of *Hurricane Isabel* (2003). Part I: Initialization, maximum winds, and the outer core boundary layer. *Mon. Weather Rev.* **137**: In press.
Nolan DS, Zhang JA, Stern DP. 2009b. Evaluation of planetary boundary layer parameterizations in tropical cyclones by comparison of in-situ observations and high-resolution simulations of *Hurricane Isabel* (2003). Part II: Inner core boundary layer and eyewall structure. *Mon. Weather Rev.* **137**: In press.
Powell MD, Uhlhorn EW, Kepert JD. 2009. Estimating maximum surface winds from hurricane reconnaissance measurements. *Weather Forecasting* **24**: 868–883.
Schwendike J, Kepert JD. 2008. The boundary layer winds in *Hurricane Danielle* 1998 and *Hurricane Isabel* 2003. *Mon. Weather Rev.* **136**: 3168–3192.
Shafran PC, Seaman NL, Gayno GA. 2000. Evaluation of numerical predictions of boundary layer structure during the Lake Michigan ozone study. *J. Appl. Meteorol.* **39**: 412–426.
Shin S, Smith RK. 2008. Tropical-cyclone intensification and predictability in a minimal three-dimensional model. *Q. J. R. Meteorol. Soc.* **134**: 1661–1671.
Smith RK. 2006. Accurate determination of a balanced axisymmetric vortex. *Tellus* **58A**: 98–103.
Smith RK, Vogl S. 2008. A simple model of the hurricane boundary layer revisited. *Q. J. R. Meteorol. Soc.* **134**: 337–351.
Smith RK, Montgomery MT. 2008. Balanced boundary layers in hurricane models. *Q. J. R. Meteorol. Soc.* **134**: 1385–1395.
Smith RK, Montgomery MT. 2010. Hurricane boundary-layer theory. *Q. J. R. Meteorol. Soc.* In press.
Smith RK, Montgomery MT, Zhu H. 2005. Buoyancy in tropical cyclone and other rapidly rotating atmospheric vortices. *Dyn. Ocean Atmos.* **40**: 189–208.
Smith RK, Montgomery MT, Nguyen SV. 2009. Tropical cyclone spin-up revisited. *Q. J. R. Meteorol. Soc.* **135**: 1321–1335. (M3).
Stull RB. 1988. *An Introduction to Boundary Layer Meteorology*. Kluwer: Dordrecht; 680 pp.
Therry G, Lacarrere P. 1983. Improving the eddy kinetic energy model for planetary boundary layer description. *Boundary-Layer Meteorol.* **25**: 63–88.
Troen IB, Mahrt L. 1986. A simple model of the atmospheric boundary layer; sensitivity to surface evaporation. *Boundary-Layer Meteorol.* **37**: 129–148.
Vogl S, Smith RK. 2009. A simple model of the hurricane boundary layer revisited. *Q. J. R. Meteorol. Soc.* **135**: 337–351.
Willoughby H. 1988. The dynamics of the tropical cyclone core. *Aust. Meteorol. Mag.* **36**: 183–191.
Willoughby HE. 1995. 'Mature structure and evolution'. In *Global Perspectives on Tropical Cyclones. WMO/TD-No 693*, Elsberry RL (ed). World Meteorological Organization: Geneva; pp 21–62.
Zhang D-L, Anthes RA. 1982. A high-resolution model of the planetary boundary layer – sensitivity tests and comparisons with SESAME-79 data. *J. Appl. Meteorol.* **21**: 1594–1609.
Zhang D-L, Liu Y, Yau MK. 2001. A multi-scale numerical study of Hurricane Andrew (1992). Part IV: Unbalanced flows. *Mon. Weather Rev.* **129**: 92–107.
Zhang JA, Marks FD, Montgomery MT, Lorsolo S. 2010. Estimation of turbulence characteristics of eyewall boundary layer of Hurricane Hugo (1989). *Mon. Weather Rev.* Submitted.

